Formation of planar structures with InGaN layers for red wavelength light sources

© D.N. Lobanov[1], M.A. Kalinnikov[1], K.E. Kudryavtsev[1], B.A. Andreev[1], P.A. Yunin[1], A.V. Novikov[1], E.V. Skorokhodov[1], Z.F. Krasilnik[1,2]

[1] Institute for Physics of Microstructures Russian Academy of Sciences, 603950 Nizhny Novgorod, Russia
[2] Lobachevsky State University of Nizhny Novgorod, 603950 Nizhny Novgorod, Russia

E-mail: dima@ipmras.ru

Received July 9, 2025
Revised October 1, 2025
Accepted October 16, 2025

Compared to the well-mastered blue-green range, the formation of InGaN-based structures that effectively emit and are photosensitive in the red and infrared wavelength ranges is a difficult task for existing growth technologies. Lowering the growth temperature is the main way to increase the In content in the InGaN solution and reduce composition fluctuations, but this can lead to degradation of the crystalline quality and radiative properties of the resulting layers. In the MBE PA method, in addition to temperature, the growth processes can be significantly influenced by changing the stoichiometric ratios of the different InGaN components. In this paper, we study the effect of growth temperature, the ratio of fluxes of III and V group elements on the formation features of planar structures with InGaN layers, their structural perfection and radiative properties in the red wavelength range. It is found that under growth conditions close to stoichiometric, a decrease in the growth temperature to 575 °C allows increasing the efficiency of In incorporation and increasing its content in InGaN to 42 %. However, in this case, composition fluctuations in the InGaN layers increase significantly, and the surface roughness and density of threading dislocations increase. It is demonstrated that at high growth temperatures of $\sim 605\,^{\circ}$C, an increase in the In flux compensating for its desorption from the growth surface allows obtaining a homogeneous InGaN layer with an In content of up to $\sim 33.5\,\%$ and smooth surface.

Keywords: indium gallium nitride, molecular beam epitaxy, red wavelength range.

DOI: 10.61011/SC.2025.07.62472.8371

1. Introduction

InGaN-based semiconductor heterostructures (GaN with a small fraction of InN) occupy leading positions in LED and laser applications in the short-wavelength, blue-green part of the visible spectrum [1–3]. The progress towards long wavelengths, into the red-orange range and further to the infrared (IR) region of the spectrum is hindered by the technological difficulties of obtaining InN and InGaN ternary solutions with a In content of $> 30\,\%$. For this reason, red-band emitters are based on the AlInGaP system, and even in full-color microdisplays based on GaN, the red color currently is „covered“ by AlInGaP pixels, which is a problem for monolithic integration of such systems. The implementation of fully III-nitride displays is an urgent task requiring the development of efficient red InGaN micro-LED. The replacement of phosphides with nitrides as sources of the red range is already being considered for microdisplays and virtual (or augmented) reality glasses. One of the problems of phosphides is the high rate of surface recombination, which is significantly aggravated when the size of light-emitting devices is reduced to micron sizes and leads to a sharp decrease in the quantum efficiency of their operation. Nitrides have a less pronounced problem, which may lead to greater efficiency of their operation compared to phosphides for micron-sized chips [4]. The well-developed technology for forming high-quality GaN epitaxial layers on silicon substrates is usually mentioned among the traditional advantages of nitrides over $A^{III}B^{V}$ materials, which not only reduces the cost of production, but also allows the integration of nitrides with silicon electronics and photonics. Another advantage is the environmental safety of nitrides compared to the production of structures based on $A^{III}B^{V}$ containing extremely toxic phosphorus and arsenic.

The main problems of advancing nitrides into the red and IR ranges are associated with an increase in the mismatch of lattice parameters between the GaN buffer layers and InGaN layers with an increase in the In content in them, as well as the need to reduce the growth temperature to increase the In incorporation coefficient in the growing InGaN layer, which leads to an increase in the defectiveness of the resulting structures [1–7]. In addition, as we move towards solutions of „medium“ InGaN compounds, the problem of phase decomposition of this compound worsens and the surface roughness increases. All of the above has led to the lack of commercial light sources based on this material in the red and IR ranges [4]. Thus, obtaining homogeneous InGaN layers with an In content of up to 50 % and an atomically smooth surface, demonstrating high crystalline

quality and radiative characteristics, is an urgent task for creating effective sources of the red wavelength range.

The motivation of the study is also related to the fact that the authors of this work were the first to obtain stimulated emission (SE) in planar structures with InN and InGaN (with In content > 60 %), grown by molecular beam epitaxy with plasma nitrogen activation (PA-MBE) [8–10]. The high density of threading dislocations in InGaN is one of the main factors determining the low temperature ($T < 200$ K) and high thresholds for the realization of stimulated radiation. It was shown in Refs. [11,12] that a decrease in the density of threading dislocations is an important factor for increasing the efficiency of spontaneous and stimulated radiation in the IR range from InN. One of the ways to reduce the density of threading dislocations is to form buffer layers that reduce the mismatch of lattice parameters between the substrate and the active layer. Thus, the growth of high-quality InGaN buffer layers with a low In content and emitting in the blue range by gas-phase epitaxy methods made it possible to form InGaN structures on them with a higher In content and improved crystalline quality, emitting in the yellow-orange wavelength range with an external quantum efficiency of up to 18 % [13]. Thus, InGaN layers of high crystalline quality with an atomically smooth surface and as high an In content as possible could serve as a buffer layer for further formation of InN-based structures on them for the IR range.

The present work is aimed at investigating the possibility of obtaining homogeneous InGaN layers of high crystalline quality and atomically smooth surface with an In content of up to 50 %.

2. Experimental procedure

The studied InGaN layers were grown on 2-inch sapphire substrates (c-Al_2O_3) using the PA-MBE method on a STE 3N3 installation (CJSC „NTO"). High-temperature buffer layers of AlN (200 nm) and GaN (700 nm) were sequentially grown on a sapphire substrate at temperatures (T_g) 820 and 710 °C, respectively. The substrate temperature was maintained at constant heater power. After the growth of the high-temperature GaN/AlN buffer layers, the heating power decreased, and the substrate temperature stabilized for ~ 30 minutes before InGaN growth. There were no changes in the pyrometer or thermocouple readings during the InGaN growth process. Further, the InGaN layer was grown for 2 hours at temperatures of $T_g \sim 575-605\,^\circ$C. The thickness of the InGaN layers was 490–600 nm, depending on the composition. The Ga flux did not change during the growth of all InGaN layers and amounted to $\sim 0.17\,\mu$m/h. In the first series of samples, in which the effect of growth temperature on the formation and properties of InGaN layers was studied, the In flux was $\sim 0.14\,\mu$m/h, and the flux of active nitrogen component was $\sim 0.33\,\mu$m/h. In the second series of samples, in which InGaN growth was studied at the highest considered temperature of $T_g \sim 605\,^\circ$C, the In flux varied from ~ 0.14 to $\sim 0.26\,\mu$m/h, and the nitrogen flux ranged from ~ 0.33 to $\sim 0.45\,\mu$m/h.

For comparison with the results of other studies, in which other units of measurement of flows were indicated, well-known geometric relationships were used. The concentration of Ga atoms for GaN in a wurtzite type lattice is $4.38 \cdot 10^{22}$ atom/cm^3 [14]. 1 ML (monolayer) of GaN corresponds to $c/2 = 0.259$ nm or $\sim 1.14 \cdot 10^{15}$ atom/cm^2 [15]. Thus, for the flux of Ga atoms $1\,\mu$m/h $= 1.22 \cdot 10^{15}$ atom/cm$^2 \cdot$ s.

To create a flux of activated nitrogen, a plasma source RF Atom Source HD 25 (Oxford Applied Research) was used; the nitrogen flow during growth did not change at 2 sccm (standard cubic centimeters per minute), the discharge power of the nitrogen plasma source varied in the range of 170–220 W. The grown samples were characterized by X-ray diffraction (XRD) using a Bruker D8 Discover diffractometer, a Keyence VHX-1000E digital optical microscope, scanning electron microscopy (SEM) using a Supra 50VP microscope, photoluminescence spectroscopy, and the Hall effect. The dislocation density was determined from the half-width of diffraction peaks detected during scanning in the directions (0004) and $(10\bar{1}2)$, in accordance with the method described in Ref. [16]. To determine the composition of the InGaN layers, maps of the reverse space were taken, since incomplete relaxation of elastic stresses was detected in them. The residual elastic stresses ranged from ~ 50 % for InGaN layers grown at 605 °C to ~ 30 % for InGaN layers grown at 575 °C. The concentration of electrons, according to Hall effect measurements, in the studied samples was $\sim 10^{17}$ cm^{-3}. The samples were excited for PL measurements by a continuous wave laser (CW) operating at a wavelength of 450 nm. The radiation of the sample was analyzed by a lattice monochromator and detected using a silicon CCD array (Princeton Instruments).

3. Models of growth processes

When considering the effect of growth temperature on the composition of InGaN layers by the MBE method, only two processes are usually mentioned — desorption of In atoms from the growth surface and thermal decomposition, which implies bond breaking In-N [17,18].

The thermal decomposition is the next important process determining the composition of the growing InGaN layer. The temperature range in which InGaN layers are obtained by the PA-MBE method is usually 450–650 °C [19]. Thermal decomposition of GaN and desorption of Ga from the growth surface are not observed in this temperature range. Therefore, the InGaN composition at a given growth temperature is determined by the rates of decomposition of In-N bonds, In desorption, and the ratios of Ga, In, and active nitrogen fluxes (N^*) [17,19]. In the case of nitrogen-enriched growth conditions, the In content in the InGaN

layer will be given by

$$x_{\text{In}} = (F_{\text{In}} - F_{\text{In}}^{\text{des}})/(F_{\text{In}} - F_{\text{In}}^{\text{des}} + F_{\text{Ga}}),$$
$$F_{\text{In}}^{\text{des}} = C^{\text{In}} \exp\left(-E_a^{\text{In}}/kT\right), \quad (1)$$

where x_{In} is the proportion of In in InGaN, F_{In} and F_{Ga} are the fluxes of In and Ga entering the growth surface, $F_{\text{In}}^{\text{des}}$ is the flux of evaporating In from the growth surface. It is important to note that nitrogen-rich growth conditions are not just a condition $F_{\text{In}} + F_{\text{Ga}} - F_{\text{In}}^{\text{des}} < F_{\text{N}}$, and a more stringent condition that takes into account the partial decomposition of In-N bonds:

$$F_{\text{In}} + F_{\text{Ga}} - F_{\text{In}}^{\text{des}} + F_{\text{InN}}^{\text{dec}} < F_{\text{N}}, \quad (2)$$

where $F_{\text{InN}}^{\text{dec}}$ is the rate of decomposition of In-N bonds [19]. For the case of metal-enriched growth conditions

$$x_{\text{In}} = 1 - F_{\text{Ga}}/\left(F_{\text{N}} - F_{\text{InN}}^{\text{dec}}\right), \quad (3)$$

where the rate of decomposition of In-N bonds depends on the composition of InGaN (x_{In}) and is determined by the expression

$$F_{\text{InN}}^{\text{dec}} = C^{\text{InN}} x_{\text{In}} \exp(-E_a^{\text{InN}}/kT), \quad (4)$$

where E_a^{InN} is the decomposition activation energy InN, C^{InN} is the decomposition rate constant. As a result, the full expression for the In content in the InGaN solution for the case of metal-enriched growth:

$$x_{\text{In}} = \left(F_{\text{N}} + B - \left((F_{\text{N}} + B)^2 - 4B(F_{\text{N}} - F_{\text{Ga}})\right)^{1/2}\right)/2B,$$
$$B = C^{\text{InN}} \exp(-E_a^{\text{InN}}/kT). \quad (5)$$

There are a number of significant drawbacks to the dependence of the composition of the growing InGaN layer on the fluxes and temperature of growth described above. First, the desorption process is considered independently of the InGaN composition and the amount of In on the surface, and the activation energy of this process $E_{\text{In}}^{\text{des}}$ is assumed to be 2.49 eV [18,19], which corresponds to the evaporation of In from the metal phase. Another disadvantage is noted by the authors of the above model and is related to the dependence of E_a^{InN} on the composition of InGaN [15]. It was experimentally shown in Ref. [17] that the activation energy of InGaN decomposition monotonously varies from 3.48 for binary InN to 3.81 eV for GaN. At the same time, the authors of Ref. [19] describe the experimental data by using the composition-independent activation energy of decomposition $E_a^{\text{InN}} = 1.84$ eV. Thus, the dependences of the decomposition rate of In-N-bonds obtained by different authors on the compositions of InGaN solutions obtained in different ratios of material flows and growth temperatures lead to the fact that the composition of InGaN layers is determined largely experimentally. The results of the model described in Ref. [19] and calculated using formulas (1)–(5) will be compared in this paper with our experimental results. More comprehensive studies, including the dependence of surface roughness, crystal quality, and radiative properties on the growth conditions for InGaN „red" wavelength range layers, are presented in the literature by isolated papers. A scientific group from the A.F.Ioffe Institute of Physics and Technology demonstrated that in case of the growth by the PA-MBE method [20] significant fluctuations in composition were observed already with an increase of the average In content in InGaN from 10 to 17 %, and the width of the integrated photoluminescence signal increased significantly, demonstrating the signal from the green region of the spectrum to the red one. This highlights the difficulty of forming homogeneous InGaN solutions for the red wavelength range, which requires a In content of $\sim 40-50$ % [21].

4. Results and discussion

In this paper, the growth of InGaN layers in the first series of samples took place nominally under slightly enriched conditions (flow ratio III/V ~ 0.94). The main parameters of this series of samples and the growth conditions are shown in Table 1. If there were no processes of In re-evaporation, InGaN decomposition and phase decomposition, then one would expect the formation of a solution with a In content of ~ 45 %, according to the formula (1).

A homogeneous solution with a In content of ~ 29 % is formed as a result of growth at the highest temperature of 605 °C (sample 1), according to X-ray diffraction analysis (Figure 1, *a*). This means that only about half of the In atoms entering the growth surface were embedded in the InGaN layer, and the incorporation coefficient of In ($K_{\text{incorp}}^{\text{In}}$), calculated as the ratio of the flux of embedded In to the incident flux of In, is ~ 0.5.

Using SEM methods, it was found that sample 1 has a smooth two-dimensional InGaN layer surface, and there are no metal In droplets on it (Figure 1, *b*). It follows from this that one part of the incident In flux is embedded in InGaN, the other has evaporated, which means that the InGaN composition in this sample is determined by the rate of desorption of metallic In. Temperature decrease to

Table 1. Main parameters of the studied structures with InGaN layers of the first series

Sample No.	T_g, °C	x_{In}, %	N_{D}, cm^{-2}	$K_{\text{incorp}}^{\text{In}}$	Droplets of In
1	605	29	$8.9 \cdot 10^{10}$	0.5	None
2	595	35	$9.5 \cdot 10^{10}$	0.65	None
3	585	37	$1.8 \cdot 10^{11}$	0.71	Present
4	575	39	$2 \cdot 10^{11}$	0.78	Present

Note. The growth temperature (T_g), the proportion of indium (x_{In}) in the composition of the ternary solution, the dislocation density (N_D), the In incorporation coefficient ($K_{\text{incorp}}^{\text{In}}$), which is equal to the ratio of the fluxes of In embedded in InGaN to the growth that fell on the surface, as well as the presence of droplets of metallic In on the surface of the InGaN layer.

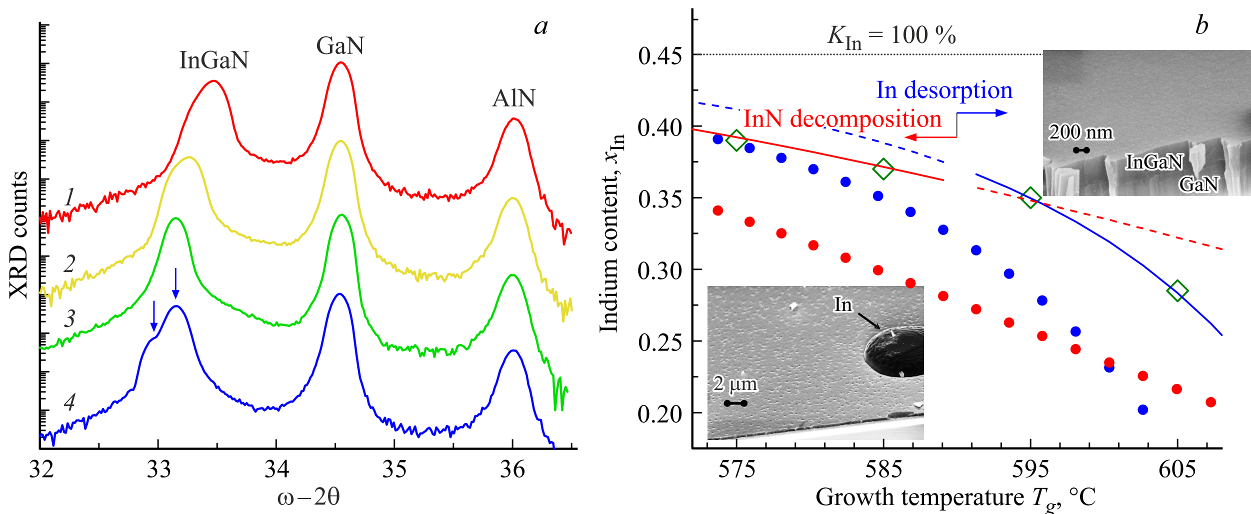

Figure 1. *a* — (0004) $\omega{-}2\theta$ X-ray diffraction spectra of samples 1, 2, 3, and 4 with InGaN layers grown at different temperatures are shown in Table 1 (curve numbers correspond to sample numbers). The blue arrows for sample 4 show InGaN signals with different contents of In (39 % — main peak, right and 43 % — „arm", to the left of the main peak). The GaN and AlN reflexes correspond to the buffer sublayers. *b* — temperature dependence of InGaN composition: green diamonds — experimental data for samples 1, 2, 3 and 4; red circles — calculation of InGaN composition under conditions of metal-enriched growth (according to (3)), with C^{InN} and E_a^{InN}, taken from Ref. [19]; blue circles — calculation of InGaN composition under conditions of nitrogen-enriched growth (according to (1)), with C^{In} and E_a^{In}, taken from Ref. [17]; red line (solid and dashed) — calculation of InGaN composition under conditions of metal-enriched growth (according to (3)), with C^{InN} and E_a^{InN} specified in this paper; blue line (solid and dashed) — calculation of InGaN composition under conditions of nitrogen-enriched growth (according to (1)), with C^{In} and E_a^{In} specified in this paper. SEM images of samples 1 (top right) and 4 (bottom left). The black dashed line shows the In content in InGaN (0.45 or 45 %) for the case of its complete embedding ($K_{\mathrm{incorp}}^{\mathrm{In}} = 1$ or 100 %).

595 °C (sample 2 from Table 1), according to SEM data, did not lead to the accumulation of metallic In on the surface, which also indicates a growth regime in which the amount of embedded In is limited by the rate of its desorption. In content in the sample 2 increased to 35 %, which is associated with a decrease in the rate of desorption of In with a decrease in T_g. The In evaporation rate according to Ref. [19]:

$$F_{\mathrm{In}}^{\mathrm{des}} = C^{\mathrm{In}} \exp(-E_a^{\mathrm{In}}/kT) = 3.4 \cdot 10^{28}\,\mathrm{atom/cm^2 \cdot c} \exp(-2.49\,\mathrm{eV}/kT). \quad (6)$$

Calculated according to these data, the In content in InGaN according to the formula (1) should be significantly less than that detected by X-ray diffraction analysis in samples 1 and 2 (Figure 1, *b*). In order for our experimental data on the In content in InGaN layers of samples 1 and 2 to be described by the model, it is necessary that $C^{\mathrm{In}} = 1.2 \cdot 10^{29}\,\mathrm{atom/cm^2 \cdot s}$, and $E_a^{\mathrm{In}} = 2.63\,\mathrm{eV}$ (Figure 1, *b*). A noticeable increase in the activation energy of evaporation In may be due to the fact that $E_a^{\mathrm{In}} = 2.49\,\mathrm{eV}$ describes In evaporation from the metallic phase — when a bilayer In is formed on the growth surface, and its excess is formed in metal droplets [18]. E_a^{In} can increase when < 2 In ML is on the surface. It is known from the literature that the activation energy of Ga evaporation from the GaN surface varies depending on the thickness of the Ga adlayer from 0 to ~ 2 ML, from 3.7 to 3.1 eV [22]. Namely, during the formation of a Ga bilayer on the GaN surface and the „droplet" growth mode, evaporation of Ga from the GaN surface corresponds to evaporation from the metal phase. A similar transient mode for the adlayer from 0 to ~ 2 ML is also present for In, but is not considered in detail in the literature.

According to X-ray diffraction analysis, the InGaN layer in the sample 2 remained homogeneous, despite the fact that the density of threading dislocations increased. Decrease of the growth temperature to $T_g \sim 585\,°\mathrm{C}$ leads to the appearance of droplets of metallic In on the InGaN surface, which indicates the transition to the „classic" metal-enriched growth mode with the formation of a metal bilayer on the surface and the accumulation of its excess in droplets on the surface (SEM image in Figure 1, *b*). In this growth mode, the composition of the InGaN layer in the sample 3 is determined by the rate of breakage of In-N bonds using the formulas (3)−(5). X-ray diffraction analysis shows that the layer is homogeneous, and the In content in it is ~ 42 % (see Table 1). When the growth temperature drops to $T_g \sim 575\,°\mathrm{C}$, the „classic" metal-enriched growth mode with the presence of In droplets on the surface remains. Constants for calculating the rate of decomposition of In-N bonds are determined in Ref. [19]:

$$B = C^{\mathrm{InN}} \exp(-E_a^{\mathrm{InN}}/kT) = 2.55 \cdot 10^{25}\,\mathrm{atom/cm^2 \cdot c} \exp(-1.84\,\mathrm{eV}/kT). \quad (7)$$

Table 2. Main parameters of the studied structures of the second series with InGaN layers

Sample No.	In flux, μm/h	N* flux, μm/h	x_{In}, %	N_D, cm^{-2}	$K^{\mathrm{In}}_{\mathrm{incorp}}$	In droplets
1	0.14	0.33	29	$8.9 \cdot 10^{10}$	0.5	None
5	0.18	0.33	33.5	$7.3 \cdot 10^{10}$	0.5	None
6	0.23	0.33	35	$9.3 \cdot 10^{10}$	0.42	Present
7	0.23	0.45	39	$1.8 \cdot 10^{11}$	0.5	Present

Note. The In and N* fluxes entering the growth surface (T_g), the share of indium (x_{In}) in the composition of the ternary solution, the density of dislocations (N_D), the In incorporation coefficient ($K^{\mathrm{In}}_{\mathrm{incorp}}$), which is equal to the ratio of the fluxes of In embedded in InGaN to the In fluxes incident on the growth surface, as well as the presence of droplets of metallic In on the surface of the InGaN layer.

Calculated according to these data, the In content in InGaN according to the formula (5) should be less than that detected by X-ray diffraction analysis in samples 3 and 4 (Figure 1, *b*). However, in order for our experimental data to be described by the model, the activation energy $E_a^{\mathrm{InN}} = 1.84$ eV must be reduced to ~ 1.4 eV, and C^{InN} to $2.4 \cdot 10^{22}$ atom/cm$^2 \cdot$ s. The difference in our estimate of E_a^{InN} and that obtained in Ref. [19] may be due to the presence in the X-ray diffraction spectrum of sample 4 of two peaks from InGaN — the main peak corresponding to the content of In ~ 39 %, and less intense peak, corresponding to the content of In ~ 43 % (Figure 1, *a*). This indicates that the average content of In in the InGaN layer of sample 4 is slightly higher than the In content used in the calculations (In ~ 39 %). This fact will increase the value of E_a^{InN} and bring it closer to the value obtained in Ref. [19]. The appearance of two peaks in the X-ray diffraction spectrum of sample 4 can be attributed to a further shift to the region of spinodal decay with a decrease in the growth temperature [23]. Therefore, the processes of phase decay and composition fluctuations are amplified, which leads to the apparent appearance of InGaN signals of different compositions in the sample 4.

As a result of studies of a series of InGaN samples (flux ratio III/V ~ 0.94) grown with a temperature change, it was found that a decrease in the growth temperature leads to degradation of their crystalline quality, despite the fact that there is a slight increase in the In content in the InGaN layers (see Table 1). Moreover, the surface roughness of InGaN layers increases (SEM images in Figure 1, *b*) with a decrease in the growth temperature according to SEM data even in case of growth in metal-enriched conditions (with the presence of In droplets on the surface).

The next series of InGaN-layered samples was grown at the highest temperature of 605 °C to ensure the high crystal quality of InGaN. In addition, intensive evaporation of In at temperatures of ~ 600 °C and above allows for growth in metal-enriched conditions, which helps to obtain an atomically smooth surface without the formation of droplets of metallic In on the growth surface. As we defined above, at this temperature, the composition of the InGaN layer is determined by evaporation of In from the growth surface. In this series of samples, we increased the In flux to determine how far it is possible to advance into the field of compositions with an In content of 40–50 %, necessary for sources of the red wavelength range. The transition from the nominally nitrogen-rich conditions in sample 1 to the nominally metal-rich conditions of sample 4 (the ratio of incident fluxes III/V~ 0.94 and 1.06) led to a significant increase in the In content in the InGaN layer from 29 to 33.5 % (Table 2).

At the same time, no droplets of metallic In are observed on the surface of sample 5. Consequently, we are still in a regime where the composition is determined by the desorption of In from the growth surface. An increase in the ratio of fluxes III/V to ~ 1.2 increased the In content in InGaN to 35 % (Table 2). Moreover, the appearance of droplets of metallic In on the InGaN surface was detected using an optical microscope (see the inset in Figure 2, *b*).

The appearance of droplets of metallic In indicates that the flux of In falling onto the surface exceeds the rate of its desorption ($F^{\mathrm{des}}_{\mathrm{In}}$). The flux of a non-embedded In is defined by the expression $F_{\mathrm{In}}(1 - K^{\mathrm{In}}_{\mathrm{incorp}})$. For sample 5, the value of this expression is less than $F^{\mathrm{des}}_{\mathrm{In}}$, and for sample 6 it is greater than $F^{\mathrm{des}}_{\mathrm{In}}$. This means that $0.08\,\mu$m/h $< F^{\mathrm{des}}_{\mathrm{In}} < 0.14\,\mu$m/h. If we calculate $F^{\mathrm{des}}_{\mathrm{In}}$ using the formula (6) for a temperature of 605 °C, we get $F^{\mathrm{des}}_{\mathrm{In}} \sim 0.11\,\mu$m/h, which coincides well with the data we obtained. And the constants C^{In} and E_a^{In} obtained in Ref. [19] well describe the In desorption in the case of the formation of droplets of metallic In on the growth surface, i. e. from the metallic phase.

The compositions of the InGaN layers in samples 5 and 6 are similar, their growth took place at the same temperature, therefore, it can be assumed that from the point of view of the thermodynamic instability of the solid solution, the phase decay processes in them should also proceed with the same intensity [23]. However, these processes were clearly manifested only in sample 6 as an additional signal from the InGaN phase with In content of ~ 42 % (Figure 2, *a*). It is assumed that the surface diffusion of adatoms, responsible for material redistribution and phase decay, is significantly accelerated for nitrides during truly metal-enriched growth, when a bilayer of metal atoms forms on the surface [24]. Bulk diffusion during epitaxial growth of semiconductor crystalline films is usually neglected [25].

With an increase in the active nitrogen flux (F_{N}) in sample 7 by ~ 1.5 times compared with sample 6, the In

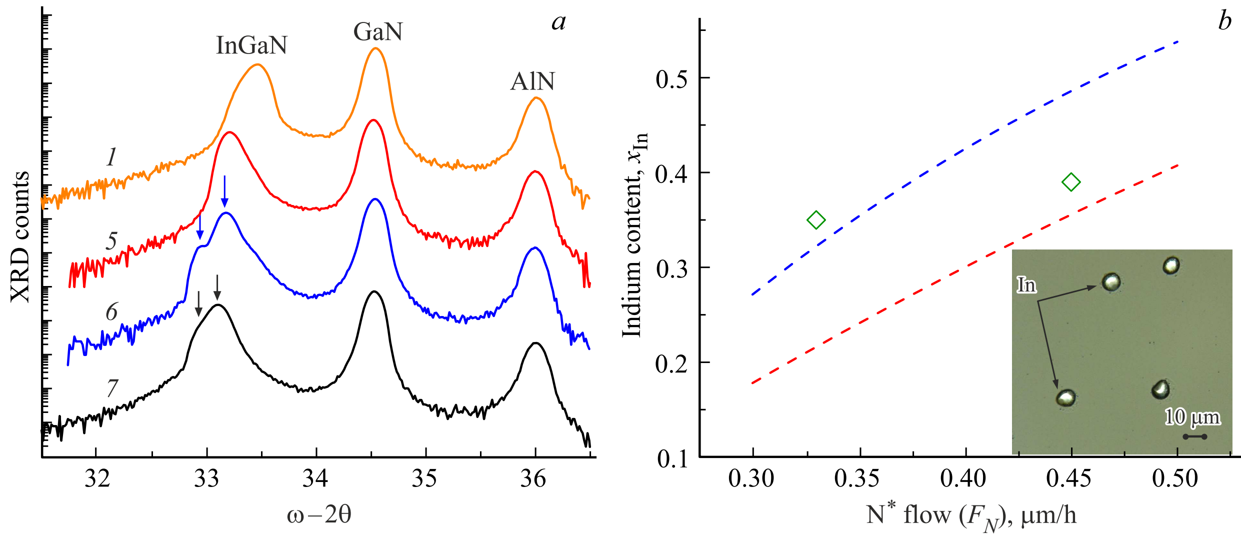

Figure 2. *a* — (0004) $\omega-2\theta$ X-ray diffraction spectra of the second series of samples from Table 2 (curve numbers correspond to sample numbers). The GaN and AlN reflexes correspond to the buffer sublayers. The arrows for samples 6, 7 show InGaN signals with different contents of In. *b* — dependence of InGaN composition on the active nitrogen flux (F_N). Green diamonds correspond to experimental data for samples 6 and 7. Dashed line — calculation of InGaN composition under conditions of metal-enriched growth (according to (3)): blue line — with C^{InN} and E_a^{InN} specified in this paper; red line — with C^{InN} and E_a^{InN} taken from Ref. [19].

content in InGaN increases from 35 to 39% (Table 2). At the same time, metal-enriched growth conditions are preserved, as evidenced by the presence of droplets of metallic In on the surface of the InGaN layer of the sample 7. According to formulas (3)–(5), the In content in the InGaN layer was calculated for the growth temperature of 605 °C depending on the active nitrogen flux both using C^{InN} from Ref. [19], and using the value obtained in the first part of this paper (Figure 2, *b*). As can be seen from Figure 2, *b*, both curves poorly describe the experimentally observed change of In content in InGaN with an increase of F_N. A slight change in composition with a significant increase in the nitrogen flux may be associated with a sharp increase in the rate of decomposition of In-N bonds (F_{InN}^{dec}) with an increase in the In content to ~ 40% or, in other words, according to the formula (4), with a significant decrease in the activation energy of the breakage of In-N bonds. A significant increase in the rate of InGaN decomposition when approaching „medium" compositions may be associated with an increase in the enthalpy of formation of InGaN compounds of „medium" compositions due to an increase in the enthalpy of mixing of InGaN solutions [26,27]. It is also possible to notice a decrease in the rate of phase decay in sample 7 compared to sample 6 — it shows an almost uniform peak from InGaN with In content of ~ 39% with an implicit „arm"-InGaN phase with In content of ~ 43%. This may be due to a shift in growth conditions towards more nitrogen-rich ones and a decrease in the rate of surface diffusion responsible for phase decay.

When studying the photoluminescence spectra of the second series of samples (Figure 3), it was found that the peak of the PL signal shifts towards lower energies as the In content in the InGaN layer increases, which is obviously related to a decrease in the band gap [21]. An interesting result is the weak dependence of the PL peak width on the InGaN layer composition (110–120 meV at 77 K) in the In composition range of 31–42% (Figure 3). At the same time, many scientific groups observed a significant broadening of the PL spectrum as the In content in InGaN

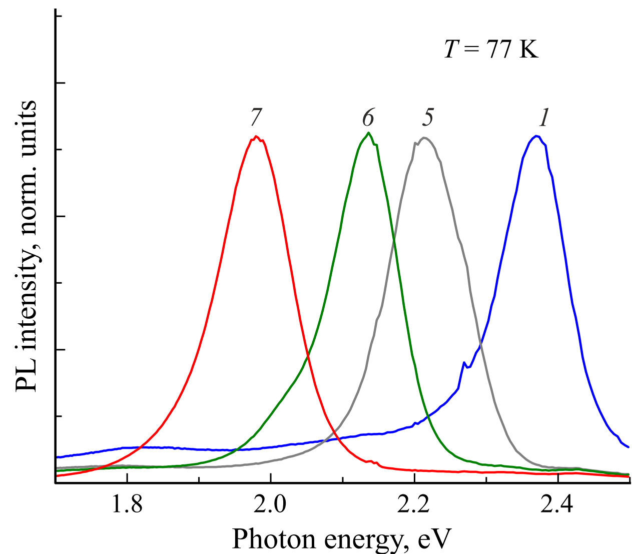

Figure 3. PL spectra of samples 1, 5, 6, 7 with InGaN layers grown at 605 °C, but with different f In and N^* fluxes from Table 2 (curve numbers correspond to sample numbers). The measurements were performed at 77 K.

increased, which was associated with increased composition fluctuations as they approached solutions of „medium" compositions [20,28]. The PL results may indicate good uniformity of the samples of the second series, despite increased fluctuations in composition in some of them (Figure 2, *a*).

5. Conclusion

Thus, the paper studies the possibility of obtaining homogeneous InGaN layers of high crystalline quality with In content up to 50 % by PA-MBE method. A decrease in the growth temperature makes it possible to increase the In content in InGaN solutions, but it leads to an increase in the density of threading dislocations and an increase in surface roughness. It has been shown that when T_g is reduced to $\sim 585\,^\circ$C, homogeneous InGaN solutions with an In content of up to 37 % can be obtained. A further decrease in the growth temperature to $T_g \sim 575\,^\circ$C leads to an increase in the processes of phase decay and the formation of an heterogeneous InGaN solution.

An increase in the In flux for the highest of the $T_g \sim 605\,^\circ$C considered in this paper allows the formation of homogeneous InGaN solutions with an In content of up to ~ 33.5 %, demonstrating an intense PL signal and a smooth two-dimensional surface. The possibility of increasing the In content in InGaN at $T_g \sim 605\,^\circ$C to ~ 35 % has been demonstrated due to an even greater increase in the In flux, however, droplets of excess metallic In and fluctuations in the composition of such an InGaN solution are observed on the growth surface. An increase in the nitrogen flux by ~ 1.5 times increases the embedding of In and its content in InGaN to ~ 39 % for $T_g \sim 605\,^\circ$C and reduces the heterogeneity of the resulting InGaN solution.

Funding

This study was carried out under the state assignment of the Institute of Physics of Microstructures, Russian Academy of Sciences FFUF-2024-0019.

Conflict of interest

The authors declare that they have no conflict of interest.

References

[1] R. Kour, S. Arya, S. Verma, A. Singh, P. Mahajan, A. Khosla. ECS J. Solid State Sci. Technol., **9**, 015011 (2020). DOI: 10.1149/2.0292001JSS

[2] Z.C. Feng. *Handbook of Solid-State Lighting and LEDs* (Boca Raton, FL, CRC Press, Taylor & Francis Group, 2017) p. 3. DOI: 10.1201/9781315151595

[3] F. Roccaforte, M. Leszczynski. *Nitride Semiconductor Technology Power Electronics and Optoelectronic Devices* (Wiley-VCH Verlag GmbH & Co. KGaA, 2020) p. 254.

[4] Ray-Hua Horng, Chun-XinYe, Po-Wei Chen, Daisuke Iida, Kazuhiro Ohkawa, Yuh-RennWu, Dong-Sing Wuu. Scientific Rep., **12**, 1324 (2022). https://doi.org/10.1038/s41598-022-05370-0

[5] C. Adelmann, R. Langer, G. Feuillet, B. Daudin. Appl. Phys. Lett., **75**, 3518 (1999). DOI:/10.1063/1.125374

[6] G.B. Stringfellow. J. Cryst. Growth, **312**, 735 (2010). DOI: 10.1016/j.jcrysgro.2009.12.018

[7] H. Chen, R.M. Feenstra, J.E. Northrup, T. Zywietz, J. Neugebauer, D.W. Greve. J. Vac. Sci. Technol. B, **18**, 2284 (2000). DOI: 10.1116/1.1306296

[8] B.A. Andreev, K.E. Kudryavtsev, A.N. Yablonskiy, D.N. Lobanov, P.A. Bushuykin, L.V. Krasilnikova, E.V. Skorokhodov, P.A. Yunin, A.V. Novikov, V.Yu. Davydov, Z.F. Krasilnik. Sci. Rep., **8**, 9454 (2018). DOI: 10.1038/s41598-018-27911-2

[9] D.N. Lobanov, K.E. Kudryavtsev, M.I. Kalinnikov, L.V. Krasilnikova, P.A. Yunin, E.V. Skorokhodov, M.V. Shaleev, A.V. Novikov, B.A. Andreev, Z.F. Krasilnik. Appl. Phys. Lett., **118**, 151902 (2021). DOI: 10.1063/5.0047674

[10] D.N. Lobanov, M.A. Kalinnikov, K.E. Kudryavtsev, B.A. Andreev, P.A. Yunin, A.V. Novikov, E.V. Skorokhodov, Z.F. Krasilnik. FTP, **58** (4), 220 (2024). (in Russian). DOI: 10.61011/FTP.2024.04.58547.6357H

[11] B.A. Andreev, K.E. Kudryavtsev, A.N. Yablonskiy, D.N. Lobanov, A.V. Novikov, H.P. Liu, B. Sheng, X.Q. Wang. J. Appl. Phys., **137**, 025701 (2025). DOI: 10.1063/5.0239375

[12] H. Liu, B. Sheng, T. Wang, K. Kudryavtsev, A. Yablonskiy, J. Wei, A. Imran, Z. Chen, X. Zheng, R. Tao, X. Yang, F. Xu, W. Ge, B. Shen, B. Andreev, X. Wang. Fundamental Res., **2** (5), 794 (2022). https://doi.org/10.1016/j.fmre.2021.09.020

[13] S. Zhang, J. Zhang, J. Gao, X. Wang, C. Zheng, M. Zhang, X. Wu, L. Xu, J. Ding, Z. Quan, F. Jiang. Photonics Res., **8** (11), 1671 (2020). https://doi.org/10.1364/PRJ.402555

[14] E. Iliopoulos, T.D. Moustakas. Appl. Phys. Lett., **81**, 295 (2002). DOI: 10.1063/1.1492853

[15] G. Koblmüller, S. Fernández-Garrido, E. Calleja, J.S. Speck. Appl. Phys. Lett., **91**, 161904 (2007). DOI: 10.1063/1.2789691

[16] M.A. Moram, M.E. Vickers. Rep. Progr. Phys., **72**, 036502 (2009). DOI: 10.1088/0034-4885/72/3/036502

[17] R. Averbeck, H. Riechert. Phys. Status Solidi A, **176**, 301 (1999). https://doi.org/10.1002/(SICI)1521-396X(199911)176:1¡301::AID-PSSA301¿3.0.CO;2-H

[18] C.S. Gallinat, G. Koblmüller, J.S. Brown, J.S. Speck. J. Appl. Phys., **102**, 064907 (2007). DOI: 10.1063/1.2781319

[19] Z. Gacevic, V.J. Gomez, N. Garcıa Lepetit, P.E.D. Soto Rodrıguez, A. Bengoechea, S. Fernandez-Garrido, R. Notzel, E. Calleja. J. Cryst. Growth, **364**, 123 (2013). http://dx.doi.org/10.1016/j.jcrysgro.2012.11.031

[20] K.G. Belyaev, M.V. Rakhlin, V.N. Jmerik, A.M. Mizerov, Ya.V. Kuznetsova, M.V. Zamoryanskaya, S.V. Ivanov, A.A. Toropov. Phys. Status Solidi C, **10** (3), 527 (2013). DOI: 10.1002/pssc.201200838

[21] J. Wu, W. Walukiewicz, K.M. Yu, J.W. Ager, E.E. Haller, H. Lu, William J. Schaff. Appl. Phys. Lett., **80**, 4741 (2002). https://doi.org/10.1063/1.1489481

[22] G. Koblmüller, R. Averbeck, H. Riechert, P. Pongratz. Phys. Rev. B, **69**, 035325 (2004). https://doi.org/10.1103/PhysRevB.69.035325

[23] S.Yu. Karpov, N.I. Podolskaya, I.A. Zhmakin, A.I. Zhmakin. Phys. Rev. B, **70**, 235203 (2004). https://doi.org/10.1103/PhysRevB.70.235203

[24] G. Koblmüller, S. Fernández-Garrido, E. Calleja, J.S. Speck. Appl. Phys. Lett., **91**, 161904 (2007). https://doi.org/10.1063/1.2789691

[25] I.P. Ipatova, V.G. Malyshkin, A.A. Maradudin, V.A. Shchukin, R.F. Wallis. Phys. Rev. B, **57**, 12968 (1998). https://doi.org/10.1103/PhysRevB.57.12968

[26] B.V. L'vov, V.L. Ugolkov. Thermochimica Acta, **438**, 1 (2005). https://doi.org/10.1016/j.tca.2005.07.007

[27] R. Mohamad, A. Bere, J. Chen, P. Ruterana. Phys. Status Solidi A, **214**, 1600752 (2017). DOI: 10.1002/pssa.201600752

[28] S.A. Kazazis, E. Papadomanolaki, M. Androulidaki, M. Kayambaki, E. Iliopoulos. J. Appl. Phys., **123**, 125101 (2018). https://doi.org/10.1063/1.5020988

Translated by A.Akhtyamov